frontiers | Frontiers in Quantum Science and Technology

TYPE Original Research
PUBLISHED 29 April 2025
DOI 10.3389/frqst.2025.1546480

OPEN ACCESS

EDITED BY
Chunlei Qu,
Stevens Institute of Technology, United States

REVIEWED BY
Aneesh Ramaswamy,
Stevens Institute of Technology, United States
Jabir Chathanathil,
United States Army Research Laboratory, United States

*CORRESPONDENCE
Yuri Rostovtsev,
rost@unt.edu

RECEIVED 16 December 2024
ACCEPTED 27 March 2025
PUBLISHED 29 April 2025

CITATION
Emerick J, Patnaik AK and Rostovtsev Y (2025) The refractive index of a single three-level atom experienced by a single photon.
Front. Quantum Sci. Technol. 4:1546480.
doi: 10.3389/frqst.2025.1546480

The refractive index of a single three-level atom experienced by a single photon

Jacob Emerick[1,2], Anil K. Patnaik[1] and Yuri Rostovtsev[1,2]*

[1]Air Force Institute of Technology, Wright-Patterson Air Force Base, Denton, OH, United States, [2]Center for Nonlinear Sciences and Department of Physics, University of North Texas, Denton, TX, United States

We study the propagation of a quantum field composed of a few photons interacting with a three-level Λ-atom driven by a coherent classical field. The quantum field acquires a phase shift, which can be interpreted as a dispersion effect on the photon wave packet and described by the refractive index for quantum fields down to the single-photon level. In this paper, we demonstrate that the phases acquired by quantum fields depend on the number of photons in the quantum states. Notably, the phases differ between single- and two-photon states, enabling the separation of multiphoton states. This finding highlights new applications related to the dispersion of three-level atoms, which are important in advancing quantum information processing and enhancing quantum communication technologies. The results are crucial for long-distance quantum communication and hold potential for developing quantum field-based linear devices such as beam splitters, lenses, and quantum prisms capable of separating different components of quantum fields. The findings can have interesting applications for manipulating and assembling of multiphoton entanglement states.

KEYWORDS

photons, quantum fields, quantum optics, three-level atoms, interference, Mach–Zehnder interferometer

1 Introduction

Electromagnetic radiation consists of photons that propagate in an empty space with the speed of light. The speed of propagation can be different when the radiation beam propagates through a medium. The index of refraction has been introduced to take into account the interaction between the radiation and the medium, and the behavior of the radiation beam is determined by the index of refraction of the medium.

Optical devices like lenses and prisms enable the manipulation of classical and quantum optical beams [see, for example, work by Leonhardt (1997)]. If the optical beam contains only a few photons, the quantum state of the radiation becomes crucial. It raises the question of whether the index of refraction remains a useful concept for single-photon physics or whether it can be applied as successfully as it has been for classical optical beams [see, for example, work by Rostovtsev et al. (2023)].

In our paper, we have used the quantum photon states using the Gaussian envelopes because they are widely used in optics and combine mathematical elegance with physical practicality, providing stable, smooth, and efficient solutions for pulse generation, propagation, and manipulation. In addition, many laser systems naturally produce pulses with Gaussian envelopes, as they arise from the fundamental mode of many

optical cavities (e.g., TEM_{00} mode). Gaussian pulses are also naturally emitted in processes involving spontaneous or stimulated emission, where the gain medium supports such distributions. In particular, the Gaussian envelope was used in a model of single-photon generation based on cavity quantum electrodynamics [see, for example, work by Walther et al. (2006b) and Walther et al. (2006a)] under adiabatic and nonadiabatic conditions [see work by Utsugi et al. (2022)].

For simplicity, we consider only a one-dimension model that could be applied if we deal with a focused Gaussian beam or the radiation in a waveguide. For example, in the work by Zheng et al. (2013), a novel scheme for quantum computation is proposed using propagating photons in a one-dimensional waveguide interacting with matter qubits. Our approach is similar in that we consider one three-level Λ–atom interacting with propagating quantum fields.

The three-level atoms driven by coherent fields, as has been shown by Fleischhauer et al. (2005) and Fleischhauer and Lukin (2000), have demonstrated various coherence effects such as the electromagnetically induced transparency (Harris, 1997) that was even demonstrated for a single atom in free space in work by Slodička et al. (2010). The important feature is the control field that can strongly modify the atomic response, as well as trap and manipulate photon states in the atomic ensembles, as shown by Lukin (2003). The process of absorption and emission is related to the phase change of the quantum fields [see, for example, work by Pollnau (2018). The strong coupling between single atoms and photons leads to the nonlinear π phase shift that was shown for single fiber-guided photons interacting with a single resonator-enhanced atom by Junge et al. (2013) and Volz et al. (2014). These results open areas for efficient manipulation of quantum states of radiation.

As is also well known, multiple qubits can be encoded per photon, and the information-carrying capacity of a single photon can be vastly expanded by exploiting its multiple degrees of freedom: spatial, temporal, and polarization [as shown by Kok and Lovett (2014) and Seitz and Theuwissen (2011)]. For example, the two-qubit single-photon quantum operations have been realized in work by Schumacher (1995), and an experimental demonstration of three-qubit single-photon, linear, deterministic quantum gates that exploit photon polarization and the two-dimensional spatial-parity-symmetry of the transverse single-photon field shown by Nielsen and Chuang (2010). Long-distance quantum communications have been demonstrated by Aspelmeyer et al. (2003). It brings us to the conclusion that the propagation of single photons in different quantum states is important, for example, when studying the stability of quantum states carrying the quantum information for quantum communications. But even more, it is interesting to see whether it is possible, for example, to develop various devices to manipulate a beam of a few photons in particular quantum states to filter quantum states and/or control their propagation. One example is a plane of single atoms that can "work" as a thin lens to manipulate and control the propagation of a single photon; that is, focusing a single photon by an array of atoms allows one to localize a single photon closer to the detector to enhance detection rate. If we can control atomic states, the focusing can be controlled, too.

Our investigations involved the simulation of a quantum field consisting of a wave packet of one multimode photon or two photons interacting with a three-level Lambda-type atomic system (see Figure 1). The incident photons (in state $|\Psi_{in}\rangle = |\Psi(t \to -\infty)\rangle$, probe) interact with the atom and, after interaction, the state is $|\Psi_{out}\rangle = |\Psi(t \to +\infty)\rangle$. The dispersion depends on the relative detuning between the resonant atomic transition and frequency of the photon but can be further controlled using a classical coherent laser field (drive). We used a state vector approach in our simulation. The single photon was modeled as a linear superposition of plane-wave modes, which sum to create a Gaussian envelope. In this scheme, the phase of each mode is modified due to their relative detuning. This nonlinear process causes dispersion of the wave packet, an example of which can be seen in Figures 2, 3. In an experimental setup, the atom can be placed in one arm of a Mach–Zehnder (MZ) interferometer [see the book by Scully and Zubairy (1997)]. The photon wave packet enters through one of the input ports, is split, and then recombined before being detected at one of the output ports. The dispersion and, therefore, the interference can be controlled through interactions with the atom. In a balanced MZ setup (without an atom), the photon can exit through one of the output ports with total probability 1, as seen in Figures 8, 9. After introducing the atom and controlling the detuning, one can see a shift in the peak detection probability in one port of the MZ interferometer. Using a drive field provides additional control.

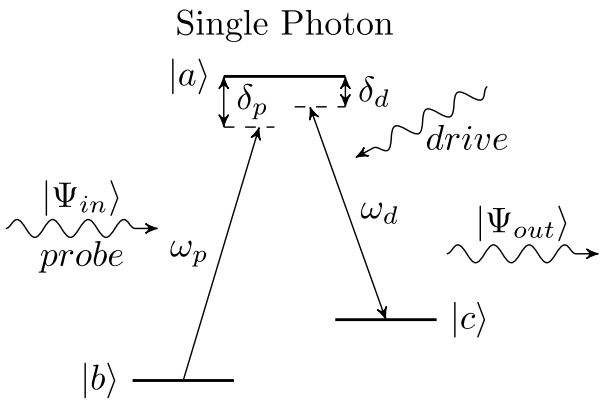

FIGURE 1
Energy levels of an atom are shown. A single incident photon ($|\Psi_{out}\rangle$, probe) with frequency ω_p is tuned to the atomic transition $|b\rangle \to |a\rangle$. Upon interacting with the atom, the photon state is changed to $|\Psi_{out}\rangle$. A classical coherent laser field (drive) with frequency ω_d is tuned to the transition $|c\rangle \to |a\rangle$. The differences between the frequencies of the incident fields and the atomic transition frequencies δ_p and δ_d are referred to as the detunings.

In the paper, we demonstrate the phase shift produced by a single atom for a single photon that can be detected by using the Mach–Zehnder interferometer. This approach allows us to show that it is possible to introduce the index of refraction for a single photon that can "work" for a broad range of applications of quantum fields: quantum information, quantum computation, imaging, and improving microscopy and long-distance quantum communication.

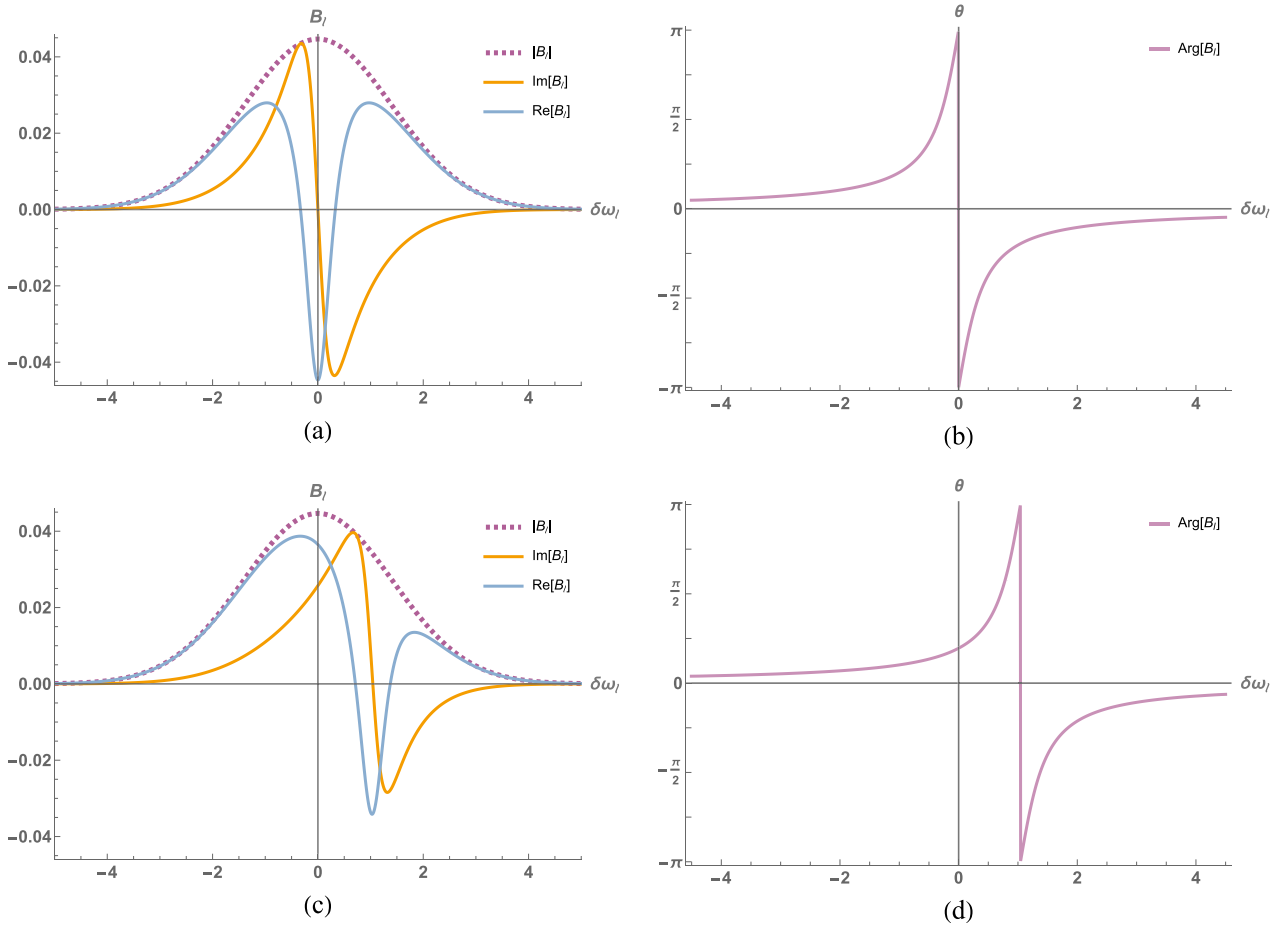

FIGURE 2
The real, imaginary parts of the probability amplitudes $B_l(t \to +\infty)$ as a function of their plane-wave mode frequency ($\delta\omega_l = \frac{(\delta_p+\delta_l)\sigma_z}{c}$) after interacting with the three-level atom. The detuning between the central Gaussian mode frequency and the atomic transition is ($\delta\omega_p = \frac{\delta_p\sigma_z}{c}$). **(a)** The Rabi frequency for the drive field ($\tilde{\Omega}_D = \frac{\Omega_D\sigma_z}{c}$) is 0, and the detuning for the drive field (δ_d) is also 0. **(b)** The argument of the $B_l(t \to +\infty)$ is shown as a function of their mode frequency. **(c)** The real, imaginary parts of the probability amplitudes $B_l(t \to +\infty)$ and **(d)** the argument of the $B_l(t \to +\infty)$ are shown for the Rabi frequency for the drive field $\tilde{\Omega}_D = \frac{\Omega_D\sigma_z}{c} = 0$, and $\delta\omega_p = 1$.

2 Methods

To take into account the propagation effects, let us consider a simple model consisting of a Lambda-type three-level atom interacting with a pulse of electromagnetic field. A clear picture of the propagation of a few photons can be obtained by employing a mode function [see the book by Kok and Lovett (2014)]. We use a wave packet for a Gaussian envelope consisting of a few photons as follows:

$$v(z,t) = \left(\frac{1}{\pi\sigma_z}\right)^{\frac{1}{4}} e^{i\left(k_p z - \omega_p t - \frac{(z-ct)^2}{2\sigma_z^2}\right)} = \sum_l \tilde{v}(k_l) e^{ik_l z - i\omega_l t}, \qquad (1)$$

where σ_z is the width of the envelope, and k_p and ω_p are the central wavenumber and the central frequency of the envelope, respectively, consisting of the frequencies $\omega_l = \omega_p + \delta_l$. Fourier modes for the Gaussian envelope are given by Equation 2.

$$\tilde{v}(k_l) = \left(\frac{\sigma_z^2}{\pi}\right)^{\frac{1}{4}} e^{-\frac{1}{2}(k_p - k_l)^2\sigma_z^2}, \qquad (2)$$

where k_l and k_p are the wavenumbers, l is the index of the spatial modes with wavenumbers k_l, ω_l, ω_p are the frequencies, L is the length of the pulse, and c is the speed of light in vacuum ($\omega_l = k_l c$ and $\omega_p = k_p c$).

Then, the field operator can be written as Equation 3:

$$\hat{E} = \sum_l \left(E_l \left(v_l(z,t)\hat{b}_l + v_l'(z,t)\hat{b}_l^+ \right) = \hat{E}^{(+)} + \hat{E}^{(-)}, \right. \qquad (3)$$

where summation over all l (the index of the spatial modes with wavenumbers k_l), $E_l = \sqrt{2\pi c\hbar k_l/V} \simeq E_0$ is the electric field per photon, V is the quantization volume, $v_l(z,t) = \tilde{v}(k_l)e^{ik_l z - i\omega_l t}$, the creation and annihilation operators obey the commutation relation [see the book by Kok and Lovett (2014)] $[\hat{b}_l, \hat{b}_l^+] = 1$, and it is convenient to introduce operators $\hat{E}^{(+)} = E_0 \sum_k v_l(z,t)\hat{b}_l$, $\hat{E}^{(-)} = E_0 \sum_l v_l'(z,t)\hat{b}_l^+$.

The state vector describing the three-level Λ atom interacting with quantum fields consisting of one- and two-photon states is given by

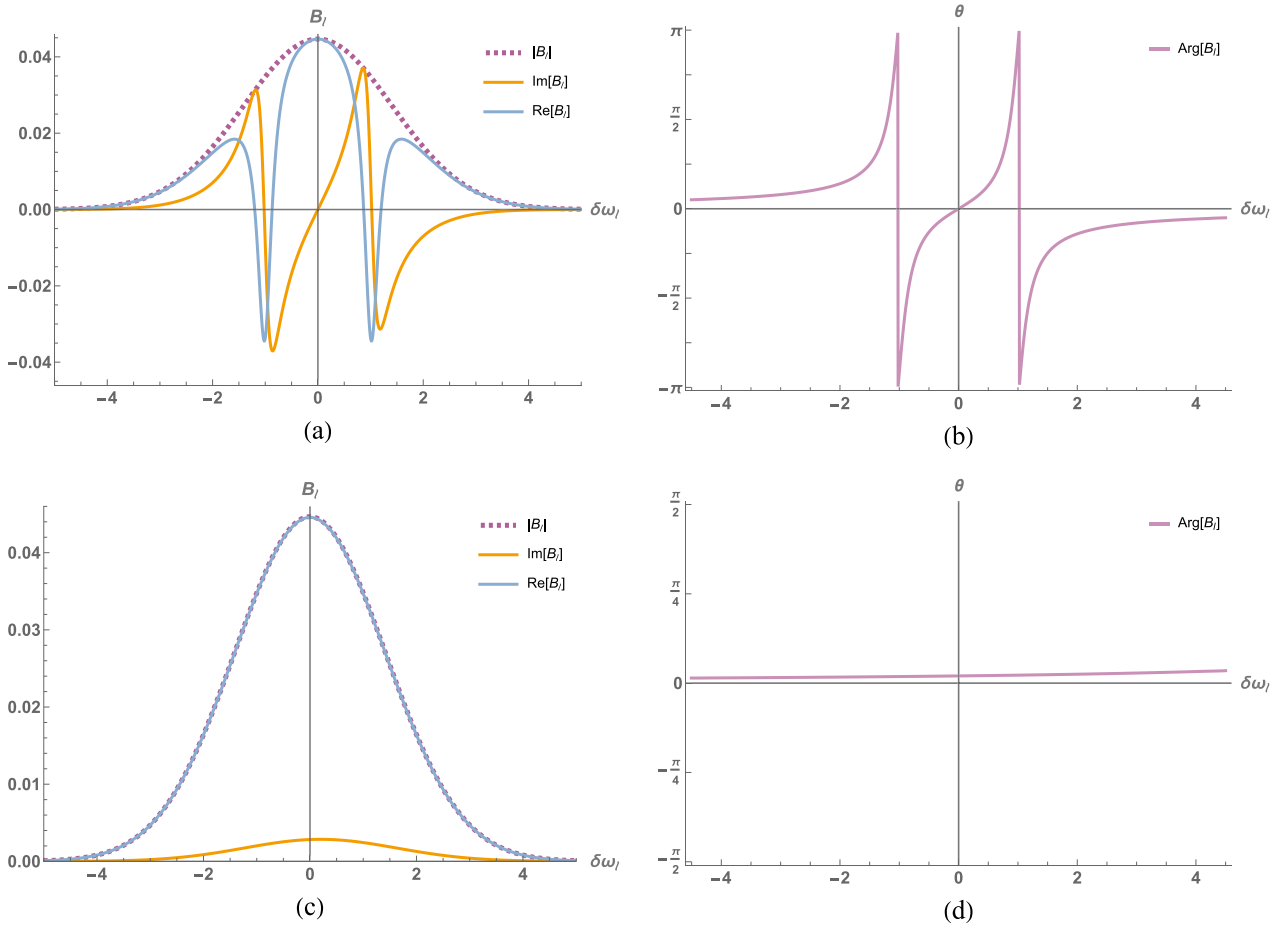

FIGURE 3
The real, imaginary parts of the probability amplitudes $B_l\,(t \to +\infty)$ as a function of their plane-wave mode frequency ($\delta\omega_l = \frac{(\delta_p+\delta_l)\sigma_z}{c}$) after interacting with the three-level atom. The detuning between the central Gaussian mode frequency and the atomic transition is ($\delta\omega_p = \frac{\delta_p\sigma_z}{c}$). **(a)** The Rabi frequency for the drive field ($\tilde{\Omega}_D = \frac{\Omega_D\sigma_z}{c}$) is 1, and the detuning for the drive field (δ_d) is 0. **(b)** The argument of the $B_l\,(t \to +\infty)$ is shown as a function of their mode frequency. **(c)** The real, imaginary parts of the probability amplitudes $B_l\,(t \to +\infty)$ and **(d)** the argument of the $B_l\,(t \to +\infty)$ are shown for the Rabi frequency for the drive field $\tilde{\Omega}_D = \frac{\Omega_D\sigma_z}{c} = 1$, and $\delta\omega_p = 10$.

$$|\Psi\rangle = A_0|a,0\rangle + \sum_l^N B_l|b,1_l\rangle + C_0|c,0\rangle + \sum_l^N A_l|a,1_l\rangle + \sum_{lq}^N B_{lq}|b,1_l,1_q\rangle + \sum_l^N B_{2l}|b,2_l\rangle + \sum_l^N C_l|c,1_l\rangle \tag{4}$$

The Hamiltonian of the atom interacting with the quantum field $\hat{E}$ and the classical field $\hat{E}_D$ is given by Equation 5:

$$\hat{V}_I = -\hat{\wp}\cdot\left(\hat{E} + \hat{E}_D\right) \tag{5}$$

where $\hat{\vec{\wp}} = \vec{\wp}_{ab}|a\rangle\langle b| + \vec{\wp}^{\star}_{ab}|b\rangle\langle a| + \vec{\wp}_{ac}|a\rangle\langle c| + \vec{\wp}^{\star}_{ac}|c\rangle\langle a|$ is the operator of the atomic dipole moment, $|a\rangle$, $|b\rangle$, and $|c\rangle$ are the states of the three-level atom, $\vec{\wp}_{ab} = q_e\langle a|\vec{r}|b\rangle$, $\vec{\wp}_{ac} = q_e\langle a|\vec{r}|c\rangle$, q_e is the electron charge, and $\omega_{ab} = (E_a - E_b)/\hbar$ and $\omega_{ac} = (E_a - E_c)/\hbar$ are the frequencies of the corresponding atomic transitions.

The interaction Hamiltonians with the quantum field and the classical fields E_D are given by Equations 6 and 7.

$$\hat{V}_{IP} = \hbar\Omega_P\sum_l^N\left(e^{i(k_lz+(\delta_l+\delta_P)t)}|a\rangle\langle b|\hat{b}_l + e^{-i(k_lz+(\delta_l+\delta_P)t)}\hat{b}_l^{+}|b\rangle\langle a|\right), \tag{6}$$

$$\hat{V}_{ID} = \hbar\Omega_D\left(e^{i\delta_d t}|a\rangle\langle c| + e^{-i\delta_d t}|c\rangle\langle a|\right), \tag{7}$$

where $\Omega_P = \wp E_0/\hbar$ and $\Omega_D = \wp E_D/\hbar$ are the Rabi frequencies describing the coupling of the quantum fields $\hat{E}$ and classical field E_D with the atom, ω_p and ω_d are the frequencies of the quantum and classical fields, and $\delta_p = \omega_{ab} - \omega_p$ and $\delta_d = \omega_{ac} - \omega_d$ are the detunings of the quantum and driving fields (see Figure 1). The state vector of the system $|\Psi\rangle$ satisfies Equation 8, the Schrodinger equation.

$$i\hbar\frac{\partial}{\partial t}|\Psi\rangle = \hat{V}_I|\Psi\rangle = \left(\hat{V}_{IP} + \hat{V}_{ID}\right)|\Psi\rangle. \tag{8}$$

Then, all A, B, and C coefficients in Equation 4 satisfy the coupled equations.

$$\dot{A}_0 = -i\Omega_P\sum_l^N\left(e^{i\left(k_lz+(\delta_l+\delta_P)t\right)}B_l\right) - i\Omega_D e^{i\delta_d t}C_0, \tag{9}$$

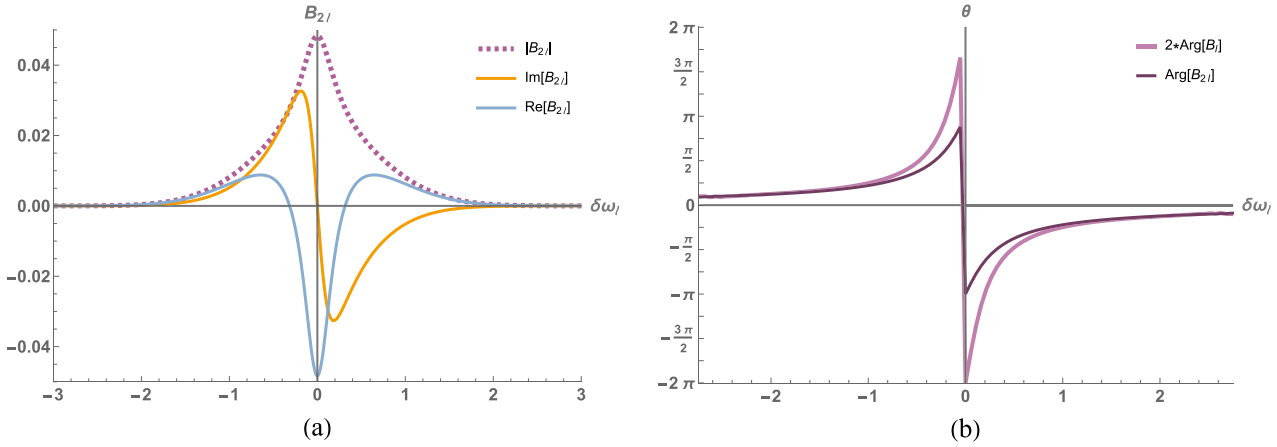

FIGURE 4
(a) The real, imaginary, and absolute value parts of the probability amplitudes $B_{2l}(t \to +\infty)$ as a function of $\delta\omega_l$ after interacting with the three-level atom. $\tilde{\Omega}_D = 0$, $\delta\omega_p = 0$. **(b)** The argument of the $B_{2l}(t \to +\infty)$ and $B_l(t \to +\infty)$ are shown as a function of their mode frequency $\delta\omega_l$.

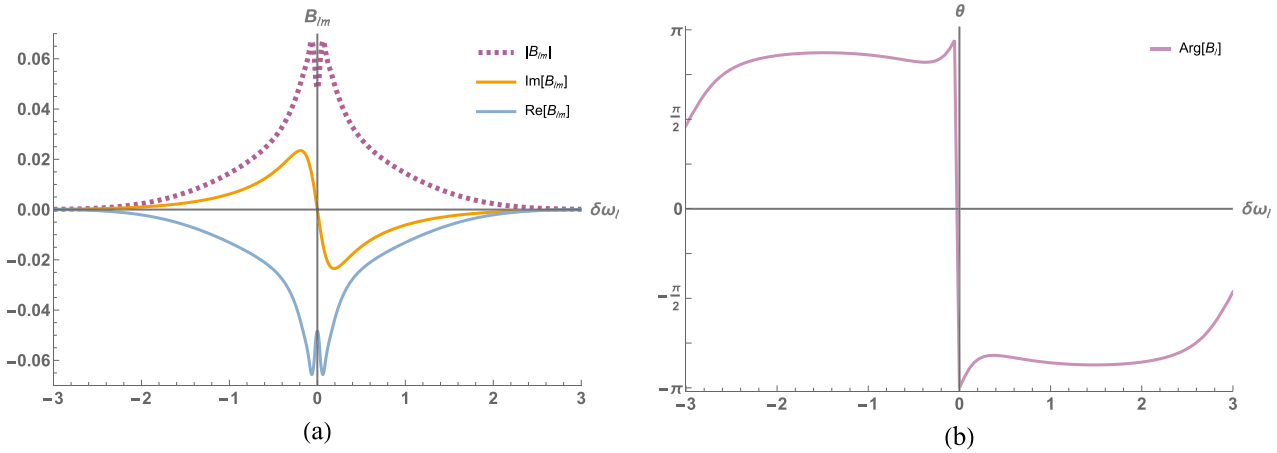

FIGURE 5
(a) The real, imaginary, and absolute value parts of the probability amplitudes $B_{lm}(t \to +\infty)$ as a function of $\delta\omega_l$ for $\tilde{\Omega}_D = 0$, $\delta\omega_p = 0$. **(b)** The argument of the $B_{2l}(t \to +\infty)$ and the double argument of the $B_l(t \to +\infty)$ are shown as a function of their mode frequency $\delta\omega_l$.

$$\dot{B}_l = -i\Omega_P e^{-i\left(k_l z + (\delta_l + \delta_p)t\right)} A_0, \tag{10}$$

$$\dot{C}_0 = -i\Omega_D e^{-i\delta_d t} A_0, \tag{11}$$

$$\dot{A}_l = -i\Omega_P \sum_q^N \left(e^{i\left(k_q z + (\delta_q + \delta_p)t\right)} B_{lq}\right) - i\sqrt{2}\Omega_P e^{i\left(k_l z + (\delta_l + \delta_p)t\right)} B_{2l} - i\Omega_D e^{i\delta_d t} C_l, \tag{12}$$

$$\dot{B}_{lq} = -i\Omega_P e^{-i\left(k_q z + (\delta_q + \delta_p)t\right)} A_l - i\Omega_P e^{-i\left(k_l z + (\delta_l + \delta_p)t\right)} A_q, \tag{13}$$

$$\dot{B}_{2l} = -i\sqrt{2}\Omega_P e^{-i\left(k_l z + (\delta_l + \delta_p)t\right)} A_l, \tag{14}$$

$$\dot{C}_l = -i\Omega_D \quad e^{-i\delta_d t} A_l. \tag{15}$$

The simulations of the set of the above equations (Equations 9–15) are presented in Figures 2–5 and reveal a variety of regimes. These include scenarios in the absence of a driving field and under the influence of the driving field. The results clearly demonstrate that introducing a driving field provides an efficient mechanism for controlling the interaction with quantum fields consisting of one- and two-photon states.

Specifically, the driving field enables precise tuning of the system's dynamics, allowing for enhanced manipulation of quantum states and greater flexibility in achieving desired outcomes. This level of control is critical for applications in quantum information processing and quantum optics, where the ability to manage photon interactions plays a key role in developing advanced technologies such as quantum sensors and single-photon sources. The simulations underscore the importance of driving fields in optimizing system performance and exploring new regimes of light–matter interaction.

2.1 Resonant interaction

At resonance, $\delta_p = 0$, we see strong effects of acquiring the phase, as can be seen in Figure 2, for $\delta\omega_p = \delta_p\sigma_z/c = 0$, $\tilde{\Omega}_D \equiv \Omega_D\sigma_z/c = 0$. A similar resonant behavior can be seen for different detunings of the probe photon and presence of drive; for example, we see the shift of the resonance for $\delta_l\sigma_z/c = 1$ and $\tilde{\Omega}_D = 0$ shown in Figure 2. After turning on the drive field, we see the Autler–Townes splitting of the transition and the strong phase acquiring for both transitions, as we can see for $\delta_p\sigma_z/c = 0$ and $\tilde{\Omega}_D = 1$ in Figure 3. For all these examples, we observe this strong phase acquiring that does not depend on the coupling with a single photon; the number of modes involved with acquiring the phase depends on the coupling. Meanwhile, we can see that if the detuning is large, for example, for $\delta\omega_p = 10$, the phase acquired for all photon modes is the same, as shown in Figure 3. Similarly, we can see the effects for two-photon mode coefficients in Figures 4, 5. We see very different behavior of photon modes. These effects require a good explanation.

Equations 9–15 describe the interaction of the system with a quantum field and also describe the relaxation of the system prepared in the excited state. These absorption and excitation processes are closely related [see work by Pollnau (2018)].

Let us first consider the relaxation that occurs when the initial condition is $A_0 = 1$. Then,

$$\dot{A}_0 = -i\Omega_P \sum_l^N \left(e^{i(k_l z+\delta_l t)} B_l\right) \tag{16}$$

$$\dot{B}_l = -i\Omega_P e^{-i(k_l z+\delta_l t)} A_0 \tag{17}$$

Consider $z = 0$, then integrating Equation 17, we obtain Equation 18,

$$B_l = -i\Omega_P \int_{-\infty}^{t} dt' A_0 e^{-i\delta_l t'} \tag{18}$$

and plugging back in Equation 16, we obtain Equation 19, the following well-known procedure [see, for example, work by Scully and Zubairy (1997)]:

$$\dot{A}_0 = -|\Omega_P|^2 \sum_l^N \int_{-\infty}^{t} dt' A_0 e^{-i\delta_l (t'-t)} = -\Gamma_0 A_0 \tag{19}$$

where D_δ is the density of states, and $\Gamma_0 = \pi D_\delta |\Omega_P|^2$ is the relaxation of the excited atomic state.

Now let us consider the atom in the ground state, $A_0 = 0$, and the photon modes are excited $B_l \neq 0$, then.

$$\dot{A}_0 = -i\Omega_P \sum_l^N \left(e^{i(k_l z+\delta_l t)} B_l\right) - \Gamma_0 A_0 \tag{20}$$

$$\dot{B}_l = -i\Omega_P e^{i(k_l z+\delta_l t)} A_0 \tag{21}$$

Then, for the amplitude of the atom in the excited state, we can write Equation 22:

$$A_0 = -i\Omega_P \sum_l e^{-\Gamma_0 t} \int_{-\infty}^{t} dt' B_l e^{(\Gamma_0+i\delta_l)t'} \tag{22}$$

Substituting Equation 22 into Equation 21 yields Equations 23 and 24:

$$\dot{B}_l = -|\Omega_P|^2 e^{-(\Gamma_0+i\delta_l)t} \sum_{l'} \int_{-\infty}^{t} dt' B_l e^{(\Gamma_0+i\delta_{l'})t'} \tag{23}$$

$$B_l(t \to +\infty) = B_l(t \to -\infty)\left(1 - \frac{2\Gamma_0}{\Gamma_0 + i\delta_l}\right), \tag{24}$$

where $B_l(t \to -\infty)$ and $B_l^0 = B_l(t \to +\infty)$ are the initial and final values for the photon field before and after interaction with the atom, respectively. Our analysis can be confirmed by comparison of our simulations with the analytical calculations presented above, as shown in Figure 6. The real and imaginary parts of B_l are plotted. Solid lines show the simulations of the equations, and dashed lines show the analytical solution given by Equation 24. The plots practically coincide. They show a very good matching of the analytical solution and our simulations, and this is an explanation for all resonant behavior on the plots shown in Figures 2, 3.

2.2 Mode function

For large detuning, when δ_p is much larger than the spectral width of the envelope, $\delta_p \gg c/\sigma_z$, where σ_z/c is the "duration" of the photon "pulse." For this case, we can see that $|\delta_p| \gg \delta_l \simeq 0$, and all modes acquire the same phase shift. Indeed, we can show this by considering for simplicity the case for $\tilde{\Omega}_D = 0$, integrating Equation 16:

$$A_0 = -\frac{\Omega_P}{\delta_p} \sum_l^N \left(e^{i(k_l z+\delta_p t)} B_l\right) \tag{25}$$

and substituting it into Equation 17:

$$\frac{\partial}{\partial t} B_1 = i\frac{\Omega_P^2}{\delta_p} \underbrace{\sum_{ll'}^N b_l^0 b_{l'}^{0*} \left(e^{i(k_{l'}-k_l)z+(\delta_{l'}-\delta_l)t}\right)}_{|V(z,t)|^2} B_1 = i\frac{\Omega_P^2}{\delta_p}|V(z,t)|^2 B_1 \tag{26}$$

$$B_1(t,z) = \exp\left(i\int_{-\infty}^{t} dt \frac{\Omega_P^2}{\delta_p}|V(z,t)|^2\right) B_1(t \to -\infty, z) \tag{27}$$

We can see indeed that all one-photon modes acquired the same phase given by Equation 27, as was also confirmed by our simulations and shown in Figure 3. The linear combination of the vacuum modes can be viewed as a photon with creation/annihilation operators defined as Equation 28:

$$\hat{B} = \sum_l^N b_l^0 \hat{b}_l \text{ and } \hat{B}^+ = \sum_l^N b_l^{0*} \hat{b}_l^+ \tag{28}$$

where b_l^0 satisfy condition $\sum_l^N |b_l^0|^2 = 1$, and the commutation relation for operators $\hat{B}$ is the same as for $\hat{b}_l$, namely, $\hat{B}\hat{B}^+ - \hat{B}^+\hat{B} = 1$. Then, the single- and two-photon states can be created by Equations 29 and 30:

$$|1\rangle = \hat{B}^+|0\rangle \text{ and } \langle 1|1\rangle = \sum_l |b_l^0|^2 = 1 \tag{29}$$

$$|2\rangle = \frac{(B^+)^2}{\sqrt{2}}|0\rangle = \sum_{l\neq q} \sqrt{2} b_l^0 b_q^0 |1_l 1_q\rangle + \sum_l (b_l^0)^2 |2_l\rangle \text{ and } \langle 2|2\rangle$$
$$= \sum_l |b_l^0|^2 \sum_q |b_q^0|^2 = 1 \tag{30}$$

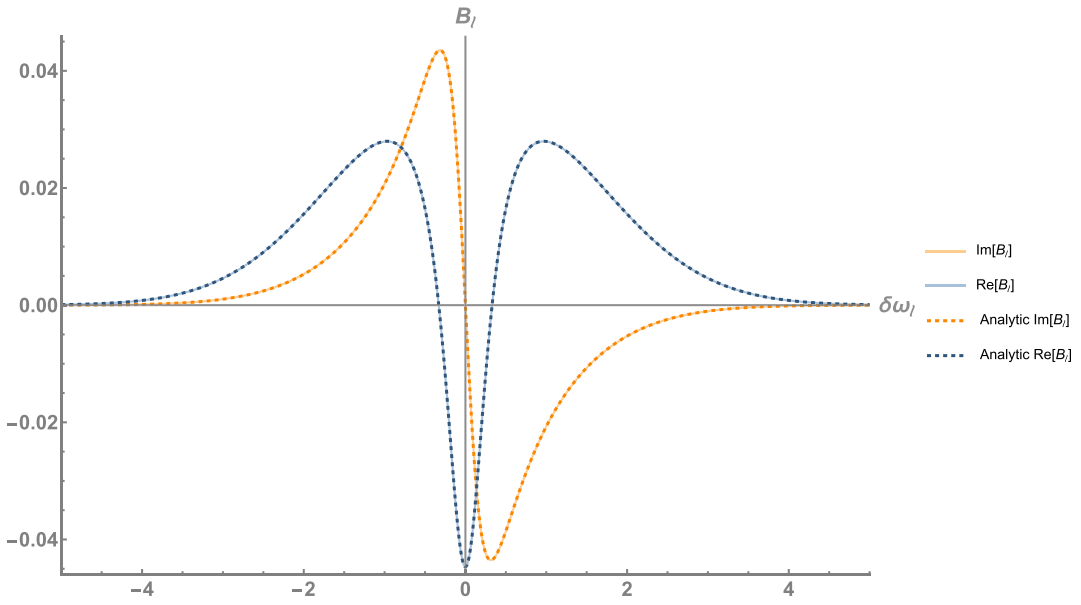

FIGURE 6
The real and imaginary parts of $B_l\,(t \to +\infty)$ are plotted. Solid lines are shown for simulations of Equations 9–15, and dashed lines are shown for analytical solutions given by Equation 24. The plots practically coincide.

Then, using the assumption that all modes acquire the same phase, $B_l = b_l^0 B_1$, we can introduce the mode function using Equation 31:

$$\sum_l^N \left(e^{i\left(k_l z+\left(\delta_l+\delta_p\right)t\right)} B_l\right) = e^{i\delta_p t} \underbrace{\sum_l^N b_l^0 e^{i(k_l z+\delta_l t)}}_{V(z,t)} B_1 = e^{i\delta_p t} V(z,t) B_1 \quad (31)$$

and $A_l = b_l^0 A_1$, $B_{lq} = \sqrt{2} b_l^0 b_q^0 B_2$, $B_{2l} = (b_l^0)^2 B_2$, and $C_l = b_l^0 C_1$

$$-i\Omega_P \sum_q^N \left(e^{i\left(k_q z+\left(\delta_q+\delta_p\right)t\right)} B_{lq}\right) - i\sqrt{2}\Omega_P e^{i\left(k_l z+\left(\delta_l+\delta_p\right)t\right)} B_{2l} = \quad (32)$$

$$-i\Omega_P \sqrt{2} e^{i\delta_p t} \left[\underbrace{\sum_{q\neq l}^N \left(e^{i\left(k_q z+\delta_q t\right)} b_l^0 b_q^0\right) + \left(e^{i(k_l z+\delta_l t)} \left(b_l^0\right)^2\right)}_{V(z,t) b_l^0}\right] B_2 \quad (33)$$

We can write for the case of a quantum field consisting of one and two photons, the state vector of the system can be written as Equation 34:

$$|\Psi\rangle = A|a,0\rangle + B_1|b,1\rangle + C|c,0\rangle + B_2|b,2\rangle + C_1|c,1\rangle \quad (34)$$

where the $A_{0,1}$, $B_{1,2}$, and $C_{0,1}$ satisfy the set of equations.

$$\dot{A}_0 = -i\Omega_P e^{ik_p z+i\delta_p t} V B_1 - i\Omega_D e^{i\delta_d t} C_0, \quad (35)$$

$$\dot{B}_1 = -i\Omega_P e^{-ik_p z-i\delta_p t} V^* A_0, \quad (36)$$

$$\dot{C}_0 = -i\Omega_D e^{-i\delta_d t} A_0 \quad (37)$$

$$\dot{A}_1 = -i\sqrt{2}\Omega_P e^{ik_p z+i\delta_p t} V B_2 - i\Omega_D e^{i\delta_d t} C_1, \quad (38)$$

$$\dot{B}_2 = -i\sqrt{2}\Omega_P e^{-ik_p z-i\delta_p t} V^* A_1, \quad (39)$$

$$\dot{C}_1 = -i\Omega_D e^{-i\delta_d t} A_1 \quad (40)$$

where $\delta_p = \omega_{ab} - \omega_p$, and $\delta_d = \omega_{ac} - \omega_d$. We obtain a system of equations that is similar to a classical three-level atom with the probe and the drive fields and can be described by the effective interaction Hamiltonian written as

$$\hat{V}_{\text{eff}} = \hbar\Omega_P \left(V(z,t) e^{i\left(k_p z+\delta_p t\right)} |a\rangle\langle b| \hat{B} + V(z,t)^* e^{-i\left(k_p z+\delta_p t\right)} \hat{B}^+ |b\rangle\langle a|\right) + \hbar\Omega_D \left(e^{i\delta_d t} |a\rangle\langle c| + e^{-i\delta_d t} |c\rangle\langle a|\right). \quad (41)$$

Under the conditions (when the probe is far detuned), the entire envelope of the photon acquires the same phase; that is, the mode function approximation works very well, as one can see in Figures 6, 4B. The important results here are also that the phase acquired by the two-photon state given by Equation 42

$$B_2(t,z) = \exp\left(2i \int_{-\infty}^t dt \frac{\Omega_P^2}{\delta_p} |V(z,t)|^2\right) B_2(t \to -\infty, z) \quad (42)$$

is exactly twice larger than the phase acquired for the one-photon state (this can be seen in Figure 4B, where the phase of the $B_{2l}\,(t \to +\infty)$ and the double phase of the $B_l\,(t \to +\infty)$ are shown as a function of their mode frequency $\delta\omega_l$. It is clearly seen that they coincide when the detuning $\delta\omega_l$ becomes large enough). This is an important result that plays an important role in the quantum state passing the Mach–Zehnder interferometer; namely, if the MZ interferometer is balanced for one far-detuned photon, it is also balanced for far-detuned two-photon modes.

2.3 Mach–Zehnder interferometer

A natural way to experimentally observe the dispersion of a single photon produced by a single atom is to use the Mach–Zehnder (MZ) interferometer shown in Figure 7. A photon has two paths for propagation; if the path is identical, the photon goes in one direction

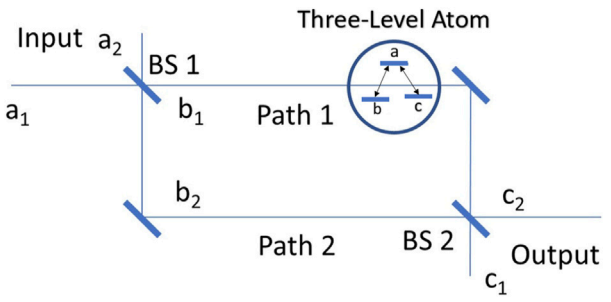

FIGURE 7
The Mach–Zehnder interferometer. The input a_1 and a_2 fields at the beam splitter BS 1, two paths: Path 1 and Path 2, for b_1 and b_2 fields combining at the beam splitter BS 2, and the output c_1 and c_2 fields. A three-level atom is located in Path 1.

with probability 1 and probability 0 at the second port of the interferometer. Meanwhile, if one path contains a single atom, it changes phases of modes and breaks the symmetry of the balanced interferometer. This results in changes in the probabilities that the photon appears at different ports of the MZ interferometer. Detecting these probabilities allows one to obtain the dispersion of the single photon during propagation through the corresponding arm of the interferometer.

The fields $\hat{a}_1$ and $\hat{a}_2$ at the input are transformed into $\hat{b}_1$ and $\hat{b}_2$ at the output of a beam splitter. We can represent in terms of state transformation S as Equation 43:

$$\begin{pmatrix} \hat{b}_1 \\ \hat{b}_2 \end{pmatrix} = \begin{pmatrix} \cos\zeta & -i\sin\zeta \\ -i\sin\zeta & \cos\zeta \end{pmatrix} \begin{pmatrix} \hat{a}_1 \\ \hat{a}_2 \end{pmatrix} = S \begin{pmatrix} \hat{a}_1 \\ \hat{a}_2 \end{pmatrix} S^{+} \tag{43}$$

where

$$S = \exp\left[i\zeta\left(\hat{a}_1^{+}\hat{a}_2 + \hat{a}_1\hat{a}_2^{+}\right)\right],$$

and ζ is the parameter of the beam splitter. Then, the output state is related to the input state as $|\text{out}\rangle = S|\text{in}\rangle$.

Let us consider an input photon state to be a one-photon state $|1,0\rangle$, then

$$|\text{out}\rangle = S|1,0\rangle = S\hat{a}_1^{+}|0,0\rangle = \cos\zeta|1,0\rangle - i\sin\zeta|0,1\rangle \tag{44}$$

Now, we can consider the MZ interferometer, which contains two beam splitters and two arms. For each beam splitter, we must calculate the output fields using Equation 44,

$$\begin{pmatrix} \hat{b}_1 \\ \hat{b}_2 \end{pmatrix} = S_1 \begin{pmatrix} \hat{a}_1 \\ \hat{a}_2 \end{pmatrix} S_1^{+}. \tag{45}$$

Then, the second beam splitter is taken into account by Equation 46:

$$\begin{pmatrix} \hat{c}_1 \\ \hat{c}_2 \end{pmatrix} = S_2 \begin{pmatrix} \hat{b}_1 \\ \hat{b}_2 \end{pmatrix} S_2^{+} \tag{46}$$

For the output state, we finally obtain Equation 47:

$$|\text{out}\rangle = MZ|1,0\rangle = S_2 U S_1|1,0\rangle = \sum_l \frac{B_l - B_l^0}{2}|1_l,0\rangle + \frac{B_l + B_l^0}{2}|0,1_l\rangle \tag{47}$$

where B_l and B_l^0 are the amplitudes before and after interaction with the atom. The underlying physics behind this phenomenon involves the interference of the photon's acquired phases due to dispersion; thus, $B_l = e^{i\phi_l}B_l^0$. The interference can result in a complete cancellation of the photon's amplitude.

In a balanced Mach–Zehnder interferometer with no obstruction in either arm, the photon wave packet can exit one of the ports with nearly 100% certainty. However, introducing an atom into one arm of the interferometer drastically alters the phase of the wave packet near the resonant transition frequency, as illustrated in Figure 2. When the central-photon frequency is detuned far from resonance, the interaction results in only a slight modification to the probability amplitude of the wave packet. This effect corresponds to an approximately uniform phase shift across all plane-wave modes within the packet, consistent with the mode function representation.

We can examine how the presence of the atom in the interferometer would affect the probability by which port (C1 or C2) the wave packet exits from the MZ interferometer. In the simulation, the balanced interferometer is constructed so that with no atom present, the photon will exist through the C1 port with probability 1. In Figure 8, we introduce the atom without a driving field, and, as a result, the probability that the wave packet leaves through the C1 port decreases. The phase of the photon wave packet is strongly modified because of the resonant interaction. As the photon is detuned from the atomic transition frequency, the phase shift is reduced. The probability that the photon will exit through the C1 port tends to 1, just as in the case where there is no atom present.

Now, we introduce a drive to the atom to see its effects on the probability of the photon. Figure 8A shows a drive ($\tilde{\Omega}_D = 1$) consistent with the probability amplitude of the photon seen in Figure 9. The introduction of the driving field splits the π-phase about the central resonant frequency. When the envelope is broad with respect to this splitting about the resonant atomic transition, there is a corresponding broadening of the probabilities of the photon seen in Figure 8B when compared to interaction without the drive. The drive is further increased in Figure 8C to $\tilde{\Omega}_D = 3$. The broadening of the probability manifests itself as two prominent peaks corresponding to the splitting of the π-phase shifts. By driving the atom, it is possible to control the probability that the photon passes through the port c_1 or c_2.

We note here that comparing the obtained results for a single atom with a few photons with the classical index of refraction given by the Maxwell equations can provide valuable insights into their behavior and interactions.

From the effective Hamiltonian given by Equation 41, assuming for a weak field that the population stays in the ground state, the atomic operator $\hat{\sigma}_{bb} - \hat{\sigma}_{aa} \simeq 1$, and then we have Equations 48, 49:

$$\frac{\partial\hat{B}}{\partial t} = -\frac{i}{\hbar}\left[\hat{V}_{\text{eff}}, \hat{B}\right] = -i\Omega_p V^{*} e^{-i\delta_p t}\hat{\sigma}_{ba} \tag{48}$$

$$\frac{\partial\hat{\sigma}_{ba}}{\partial t} = -\frac{i}{\hbar}\left[\hat{V}_{\text{eff}}, \hat{\sigma}_{ba}\right] = -i\Omega_p V e^{i\delta_p t}\left(\hat{\sigma}_{bb} - \hat{\sigma}_{aa}\right)\hat{B} \simeq -i\Omega_p V e^{i\delta_p t}\hat{B}. \tag{49}$$

Then, using the adiabatic approximation valid for the large detuning δ_p, we can obtain

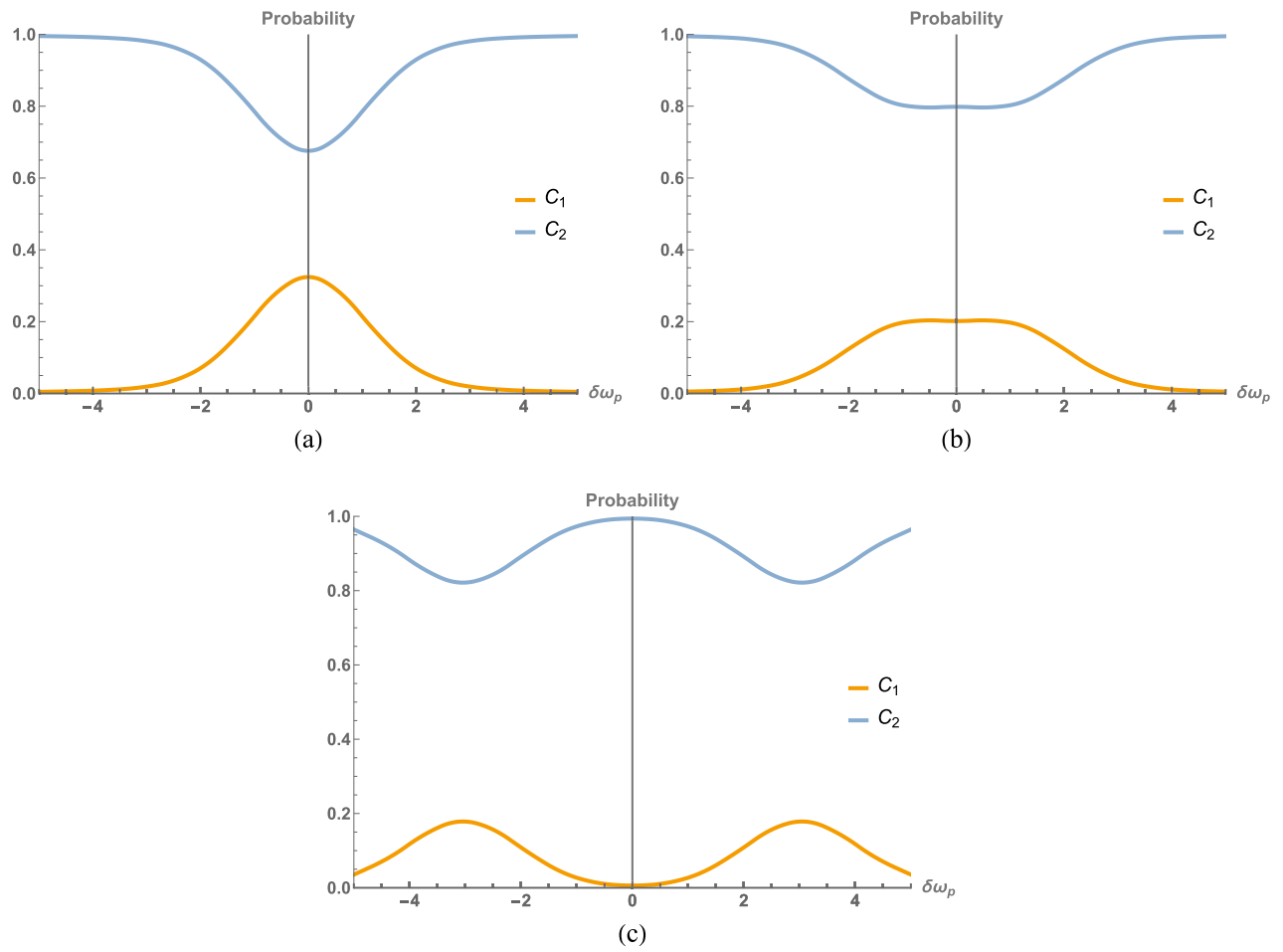

FIGURE 8
(a) Probability that the photon will exit a given port as a function of detuning from atomic transition ($\delta\omega_p$). There is no classical driving laser field present, $\tilde{\Omega}_D = 0$. **(b)** $\tilde{\Omega}_D = 1$. **(c)** $\tilde{\Omega}_D = 3$.

$$\frac{\partial \hat{B}}{\partial t} = -i\frac{\Omega_p^2}{\delta_p}|V|^2\hat{B} \tag{50}$$

where we can see that the phase factor, which appears above, coincides with the index of refraction that can be obtained from Maxwell equations for the classical field [see, for example, the book by Scully and Zubairy (1997)]. Indeed, according to Equation 50, the phase shift is given by

$$\Phi = \frac{\Omega_p^2}{\delta_p}\tau \tag{51}$$

where $\tau$is the "pulse" duration of the photon envelope. Thus, Equation 51 can be rewritten as Equation 52:

$$\Phi = k_{ab}L_\tau(n-1) = \frac{\omega_{ab}}{c}c\tau\frac{4\pi\wp_{ab}^2}{\hbar\delta_p}\frac{N}{V} \tag{52}$$

and

$$n - 1 = \frac{4\pi\wp_{ab}^2}{\hbar\delta_p}\frac{N}{V} \tag{53}$$

which is exactly the index of refraction for the weak classical field [see, for example, the book Scully and Zubairy (1997)]. For our consideration, $N = 1$ (we consider only one atom), but for considering the N atoms, we can consider a "collective" ground state $|b\rangle$ and the excited state $|a\rangle$, and we can notice that the ground states is given by $|b_c\rangle = |b_1 b_2 \ldots b_N\rangle$, meanwhile the excited state is given by Equation 54:

$$|a_c\rangle = \sum_{i=1}^{N}\frac{|b_1 b_2 \ldots a_i \ldots b_N\rangle}{\sqrt{N}} \tag{54}$$

Then, the "collective" dipole moment is given by $\wp_c = \wp_{ab}\sqrt{N}$, which gives the density of atoms in Equation 53. More details about the appearance of the "collective" factors $\sqrt{N}$ can be found in the works of Dicke (1954), Fleischhauer and Lukin (2000), and Lukin (2003). Thus, we can see that comparing the obtained results for a single atom and a few photons with the classical index of refraction provides valuable insights. We can see that even if the field has the phase shift exactly related to the "index of refraction" for classical fields guided by Maxwell equations, the quantum states can obtain the phase shift that can be used for applications such as higher

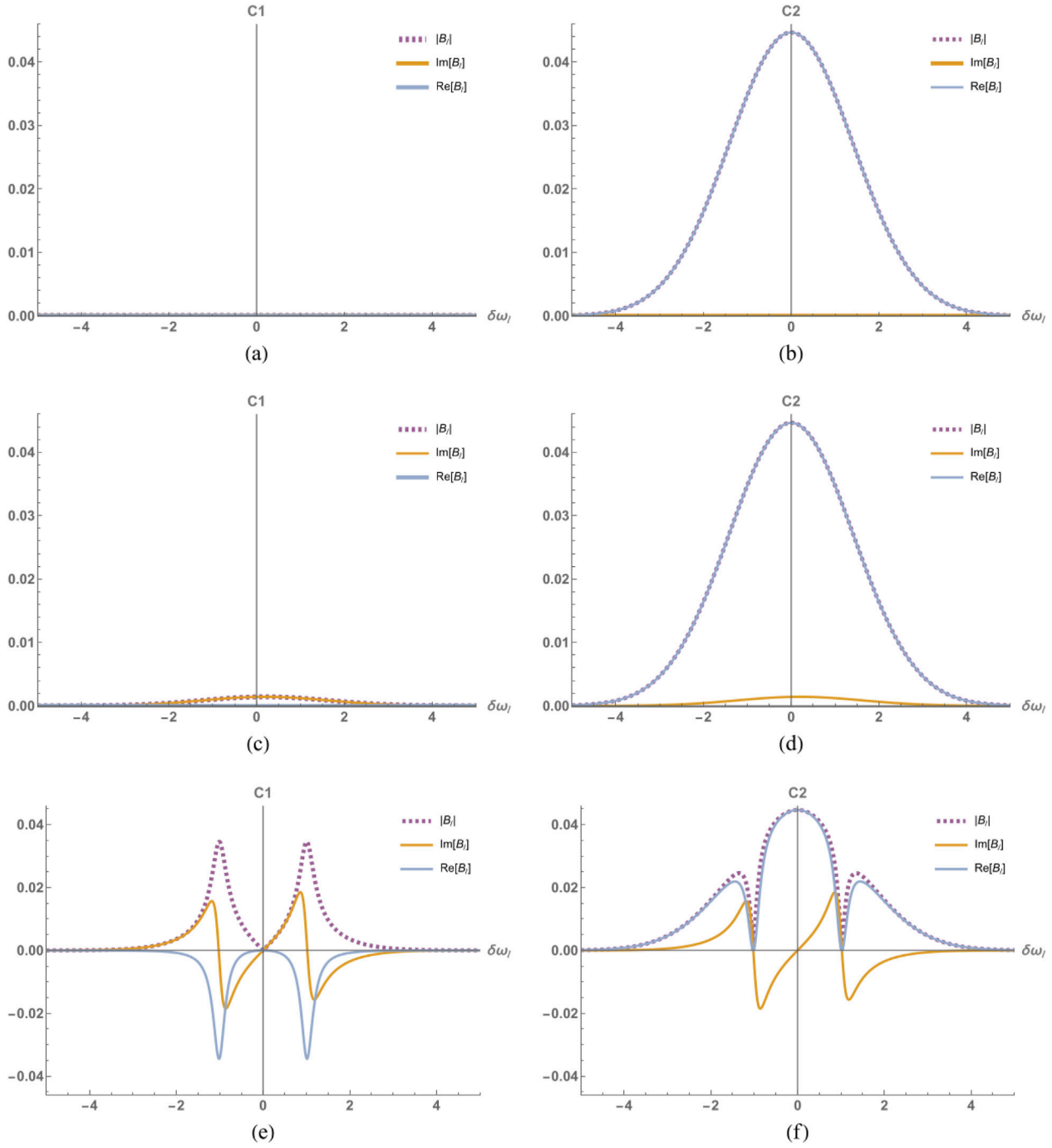

FIGURE 9
Balanced MZ interferometer with no atom present. The probability amplitude of $B_l\,(t \to +\infty)$ at the two output ports: **(a)** C1 and **(b)** C2. Balanced MZ interferometer with one atom present, no drive ($\tilde{\Omega}_D = 0$), and high detuning ($\delta\omega_l = 10$). The probability amplitude of $B_l\,(t \to +\infty)$ at the two output ports: **(c)** C1 and **(d)** C2. For driving field ($\tilde{\Omega}_D = 1$), and no detuning ($\delta\omega_l = 0$). The probability amplitude of $B_l\,(t \to +\infty)$ at the two output ports: **(e)** C1 and **(f)** C2.

spatial resolution and designing devices that can separate different quantum states.

Possible applications of the obtained results can be related to controlling the output of the MZ interferometer. In particular, with a three-level atom present in one arm of the interferometer, one can use the driving field in conjunction with a path delay phase shift to achieve a variety of desirable effects. In a simple case, the driving field can be used to toggle the MZ interferometer between a balanced configuration and a desired output so long as the photon wave packet's central frequency is close to the resonant transition frequency. If the initial photon states are unknown, one could, in principle, drive the atom to act as a filter for particular photon states. Given a known initial photon state, one could use the atom as a veritable splitter to control which port the photon would leave with adjustable probability. Given that the incident photon was in some entangled state, the atom

could be used as a scheme to perform some interaction-free measurements.

Thus, we can see that our study is focused on the dynamics of a single photon interacting with a three-level atom. We investigated various aspects related to the propagation of this photon and highlighted the significance of phase and group velocities in the context of long-distance quantum communications.

Understanding the behavior of a single photon is of great importance in quantum communication systems, where information is encoded and transmitted using quantum states. By examining the interaction between a single photon and a two-level atom, we gained insights into how the photon's properties are influenced and modified during its propagation.

By studying the dispersion of the single-photon propagation, we have deepened our understanding of the fundamental properties that govern quantum communications. These findings contribute to the development of more efficient and reliable quantum communication systems, which are crucial to the advancement of technologies such as quantum cryptography, quantum teleportation, and quantum computing.

3 Conclusion

In conclusion, we have demonstrated that the mode function can be effectively utilized in scenarios involving large detunings, highlighting its versatility and relevance in quantum systems with non-resonant interactions. Through our analysis, several useful approximations of the density matrix solution have been derived, offering valuable insights into the dynamics of such systems.

Furthermore, we have shown that the one- and two-photon resonance modes undergo significant phase shifts, which are crucial for understanding and manipulating quantum coherence and interference effects. These findings pave the way for more precise control in applications such as quantum information processing, nonlinear optics, and spectroscopy. The ability to predict and manage these phase shifts could enable the design of novel quantum devices and experiments, pushing the boundaries of what is achievable in the field of quantum optics and quantum mechanics. In particular, we describe the system of generating correlated photons.

We provide a detailed description of the system designed for generating correlated photons, emphasizing its underlying principles, mechanisms, and potential applications. The system leverages quantum coherence and nonlinearity to create photon pairs with strong temporal and spectral correlations, which are essential for various applications in quantum technologies.

By carefully controlling the interaction of optical fields with the medium, we demonstrate how the system can produce photons that are entangled or exhibit strong quantum correlations. These correlated photons play a pivotal role in advancing quantum communication protocols, such as quantum key distribution, and are fundamental resources for quantum computing and quantum sensing.

Additionally, the approach offers a platform to explore the fundamental properties of quantum light, such as photon statistics, coherence, and interference, thus contributing to a broader understanding of quantum mechanics. This system not only highlights the feasibility of generating correlated photons but also provides a foundation for the development of scalable and efficient quantum light sources for practical implementations.

Data availability statement

The original contributions presented in the study are included in the article/supplementary material; further inquiries can be directed to the corresponding author.

Author contributions

JE: investigation, methodology, validation, writing – original draft, and writing – review and editing. AP: conceptualization, investigation, methodology, project administration, supervision, writing – original draft, and writing – review and editing. YR: conceptualization, formal analysis, investigation, methodology, project administration, validation, writing – original draft, and writing – review and editing.

Funding

The author(s) declare that financial support was received for the research and/or publication of this article. AP is thankful the Directed Energy Joint Transition Office (JDETO) for the support. This paper has been cleared for public release, clearance number 88ABW-2024-1017.

Acknowledgments

We thank Girish Agarwal, Konstantin Dorfman, Billie Deluca, Keith A. Wyman, Michael Pak, David E. Weeks, and Barnabas (Moochan) Kim for fruitful discussions, comments, and suggestions. JE and YR are grateful for the support of the 2023–2024 AFOSR Summer Faculty Fellowship Programs at AFIT. AP is thankful for the AFOSR grant.

Conflict of interest

The authors declare that the research was conducted in the absence of any commercial or financial relationships that could be construed as a potential conflict of interest.

Generative AI statement

The author(s) declare that no Gen AI was used in the creation of this manuscript.

Publisher's note

References

Aspelmeyer, M., Jennewein, T., Pfennigbauer, M., Leeb, W., and Zeilinger, A. (2003). Long-distance quantum communication with entangled photons using satellites. *IEEE J. Sel. Top. Quantum Electron.* 9, 1541–1551. doi:10.1109/.jstqe.2003.820918

Dicke, R. H. (1954). Coherence in spontaneous radiation processes. *Phys. Rev.* 93, 99–110. doi:10.1103/PhysRev.93.99

Fleischhauer, M., Imamoglu, A., and Marangos, J. (2005). Electromagnetically induced transparency: optics in coherent media. *Rev. Mod. Phys.* 77, 633–673. doi:10.1103/revmodphys.77.633

Fleischhauer, M., and Lukin, M. D. (2000). Dark-state polaritons in electromagnetically induced transparency. *Phys. Rev. Lett.* 84, 5094–5097. doi:10.1103/PhysRevLett.84.5094

Harris, S. E. (1997). Electromagnetically induced transparency. *Phys. Today* 50, 36–42. doi:10.1063/1.881806

Junge, C., O'Shea, D., Volz, J., and Rauschenbeutel, A. (2013). Strong coupling between single atoms and nontransversal photons. *Phys. Rev. Lett.* 110, 213604. doi:10.1103/PhysRevLett.110.213604

Kok, P., and Lovett, B. W. (2014). *Optical quantum information processing*. Cambridge: Cambridge University Press.

Leonhardt, U. (1997). *Measuring the quantum state of light*. Cambridge, UK: Cambridge University Press.

Lukin, M. D. (2003). *Colloquium*: trapping and manipulating photon states in atomic ensembles. *Rev. Mod. Phys.* 75, 457–472. doi:10.1103/RevModPhys.75.457

Nielsen, M. A., and Chuang, I. L. (2010). *Quantum computation and quantum information*. Cambridge: Cambridge University Press.

Pollnau, M. (2018). Phase aspect in photon emission and absorption. *Optica* 5, 465–474. doi:10.1364/optica.5.000465

Rostovtsev, Y., Emerick, J., and Patnaik, A. (2023). The refractive index of a single atom experienced by a single photon. *Results Opt.* 13, 100568. doi:10.1016/j.rio.2023.100568

Schumacher, B. (1995). Quantum coding. *Phys. Rev. A* 51, 2738–2747. doi:10.1103/PhysRevA.51.2738

Scully, M. O., and Zubairy, M. S. (1997). *Quantum optics*. Cambridge: Cambridge university press.

Seitz, P., and Theuwissen, A. J. P. (2011). *Single-photon imaging* (Heidelberg: Springer-Verlag Berlin).

Slodička, L., Hétet, G., Gerber, S., Hennrich, M., and Blatt, R. (2010). Electromagnetically induced transparency from a single atom in free space. *Phys. Rev. Lett.* 105, 153604. doi:10.1103/physrevlett.105.153604

Utsugi, T., Goban, A., Tokunaga, Y., Goto, H., and Aoki, T. (2022). Gaussian-wave-packet model for single-photon generation based on cavity quantum electrodynamics under adiabatic and nonadiabatic conditions. *Phys. Rev. A* 106, 023712. doi:10.1103/physreva.106.023712

Volz, J., Scheucher, M., Junge, C., and Rauschenbeutel, A. (2014). Nonlinear π phase shift for single fibre-guided photons interacting with a single resonator-enhanced atom. *Nat. Photonics* 8, 965–970. doi:10.1038/nphoton.2014.253

Walther, H., Varcoe, B. T., Englert, B.-G., and Becker, T. (2006a). Cavity quantum electrodynamics. *Rep. Prog. Phys.* 69, 1325–1382. doi:10.1088/0034-4885/69/5/r02

Walther, H., Varcoe, B. T. H., Englert, B.-G., and Becker, T. (2006b). Cavity quantum electrodynamics. *Rep. Prog. Phys.* 69, 1325–1382. doi:10.1088/0034-4885/69/5/R02

Zheng, H., Gauthier, D. J., and Baranger, H. U. (2013). Waveguide-qed-based photonic quantum computation. *Phys. Rev. Lett.* 111, 090502. doi:10.1103/physrevlett.111.090502